

Fast ion conduction character and ionic phase-transition in silver sulfosalts: The case of fettelite $[\text{Ag}_6\text{As}_2\text{S}_7][\text{Ag}_{10}\text{HgAs}_2\text{S}_8]$

LUCA BINDI^{1,2,*} AND SILVIO MENCHETTI³

¹Museo di Storia Naturale, Sezione di Mineralogia, Università di Firenze, Via La Pira 4, I-50121 Firenze, Italy

²C.N.R., Istituto di Geoscienze e Georisorse, Sezione di Firenze, Via La Pira 4, I-50121 Firenze, Italy

³Dipartimento di Scienze della Terra, Università di Firenze, Via La Pira 4, I-50121 Firenze, Italy

ABSTRACT

The mineral fettelite, $[\text{Ag}_6\text{As}_2\text{S}_7][\text{Ag}_{10}\text{HgAs}_2\text{S}_8]$, has been recently structurally characterized. On the whole, the structure can be described as a regular succession of two module layers stacked along the *c*-axis: a first module layer (labeled *A*) with composition $[\text{Ag}_6\text{As}_2\text{S}_7]^{2-}$ and a second module layer (labeled *B*) with composition $[\text{Ag}_{10}\text{HgAs}_2\text{S}_8]^{2+}$. Here we report an integrated high-temperature single-crystal X-ray diffraction (HT-SCXRD), differential scanning calorimetry (DSC), and complex impedance spectroscopy (CIS) study on a sample of fettelite from Chañarcillo, Copiapó Province, Chile. DSC and conductivity measurements pointed out that fettelite shows a ionic-transition at about 380 K. HT-SCXRD experiments confirmed the phase transition toward a disordered phase having a trigonal symmetry with the *a* and *b* unit-cell parameters halved. In the HT-structure, the disorder is located in the *B* layer where the Ag-Hg cations are found in various sites corresponding to the most pronounced probability density function locations of diffusion-like paths. This indicates that at least two polytypes could exist for fettelite, the ordered, monoclinic RT-structure (space group *C2*), and a fast ion conducting, trigonal, disordered HT-form (space group $P\bar{3}m1$) with *a* and *b* parameters halved. The two unit-cell types (corresponding to two different polytypes) could be also found in nature. Slightly different chemical compositions for different fettelite samples (e.g., different Ag/Hg ratios) could play a crucial role as driving forces for different unit-cell stabilizations.

Keywords: Fettelite, HT-data collection, conductivity spectrum, ionic phase transition, fast ionic conductor

INTRODUCTION

It is well known that in fast ionic conductors, also called superionic conductors, an ionic species can move easily, giving rise to a liquid-like structure in an open framework (tunnels, layers, etc.). The delocalization of the moving species is favored when a low-activation energy for the jumps and similar site potential energies exists. Silver is well known to give such a high conductivity, with Ag_3SI (Reuter and Hardel 1965) and RbAg_4I_5 (Owens and Argue 1967) being among the first fast ionic conductors discovered. A reason for the high Ag mobility is the preference of d^{10} cations for low coordination, which in turn has been explained through band structure calculation by *s/d* orbital mixing and polarization factors (Gaudin et al. 2001).

Bindi et al. (2006 and references therein) showed that minerals belonging to the pearceite-polybasite group with general formula $[(\text{Ag,Cu})_6M_2\text{S}_7][\text{Ag}_y\text{CuS}_4]$ with *M* = As and Sb exhibit fast ion conductivity. These authors also elucidated the atomic structures and the ionic phase transitions of all the members of the group by means of differential scanning calorimetry (DSC) and complex impedance spectroscopy (CIS) studies and in situ single-crystal X-ray diffraction experiments. Based on these results, we have attempted to determine whether there are any minerals, strictly related to those of the pearceite-polybasite group, which could behave as fast ion conductors. Although not belonging to this group, fettelite, $[\text{Ag}_6\text{As}_2\text{S}_7][\text{Ag}_{10}\text{HgAs}_2\text{S}_8]$, bears structural similarities to members

of this group. Such a mineral, indeed, has been recently structurally characterized based on data collected from a twinned crystal from Chañarcillo, Copiapó Province, Chile (Bindi et al. 2009). It shows strong structural analogies with the minerals belonging to the pearceite-polybasite group. A detailed investigation on fettelite was then initiated, by means of conductivity and calorimetric studies and in situ single-crystal X-ray diffraction experiments. This paper reports the complete analysis of the fast ion conduction character and ionic phase transition for fettelite.

DSC AND CONDUCTIVITY MEASUREMENTS

The sample containing the fettelite crystals used in the present study (Harvard Mineralogical Museum cat. number 140586) is from Chañarcillo, Chile. A detailed description (including the chemical composition) of the sample is given by Bindi et al. (2009). DSC measurements between 193 and 423 K with a heating rate of 10 K/min were carried out on 25 mg of powder sealed in aluminum pans using a Mettler DSC 30 instrument. Conductivity measurements were performed in a home made conductivity cell with a SOLARTRON SI-1260 impedancemeter in the frequency range 1 Hz to 10 MHz. Conductivity samples were cylindrical pellets of 5 mm in diameter and approximately 1 mm in thickness. Two silver electrodes were deposited on the flat faces of the pellet by vacuum deposition. The measurements were carried out under dynamic vacuum from 210 to 400 K. Measurements below room temperature were carried out while placing the cell in a liquid nitrogen bath. For measurements

* E-mail: luca.bindi@unifi.it

above room temperature, a BUCHI TO-50 furnace was used to heat the sample. Conductivity was measured every 10°, and cycles in temperature ensured the reproducibility of the results.

In situ single-crystal X-ray diffraction

To study the hypothesized phase transition we analyzed the same sample used for the conductivity measurements. The investigated crystal was isolated from a broken sample and fixed at the tip of a glass capillary by means of solvent-free glue. The diffraction quality was initially checked by means of a Bruker-P4 single-crystal diffractometer equipped with a conventional point detector. Then, the unit-cell values were carefully measured by means of an Oxford Diffraction “Xcalibur 3” single-crystal diffractometer (enhanced X-ray source, X-ray radiation MoK α , $\lambda = 0.71073$ Å) fitted with a Sapphire 2 CCD detector. A total of 100 frames of data were collected at room temperature as 3 sets of omega runs with an exposure time of 100 s per frame and a frame width of 0.75°. Data frames were processed using the CrysAlis software package running on the Xcalibur 3 control PC. The unit-cell values found at RT (Table 1) were very similar to those given by Bindi et al. (2009) for the RT-fettelite. Moreover, we monitored the intensities of some selected hkl reflections, i.e., 151, 352, 17 3 $\bar{3}$, 736, 442, and 441, together with their equivalent reflections (Fig. 1). Subsequently, the temperature was raised to 310 K with a heating rate of 5 K/h, and the same data set was collected. The same procedure was then repeated at 320, 335, and 350 K (Table 1; Fig. 1). For a temperature of >350 K, the intensities of the selected reflections with h and $k = 2n + 1$ (i.e., 151, 352, 17 3 $\bar{3}$, 736) became too low to be measured. Thus, the temperature was raised to 400 K and a whole intensity data collection was carried out. In expectation of possible crystal twinning, a full diffraction sphere was collected. The diffraction pattern was consistent with trigonal symmetry ($a \approx 7.6$ and $c \approx 15.6$ Å), with a and b parameters halved with respect to the RT values. Intensity integration and standard Lorentz-polarization corrections were done with the CrysAlis RED (Oxford Diffraction 2006) software package. The program ABSPACK of the CrysAlis RED package (Oxford Diffraction 2006) was used for the absorption correction. The high temperatures (up to 400 K) were achieved by means of an Oxford cryostream cooler.

The unit-cell parameters are reported in Table 1. Before each measurement the sample was maintained at the specified temperature for about 30 min. As a check, the crystal was cooled to 320 K. The unit-cell values obtained did not reveal significant variations from the previous one, thus indicating that no hysteresis occurs within the temperature range examined.

Structure determination of the HT-structure

No particular systematic extinctions were observed at 400 K, allowing $P\bar{3}m1$ as a possible space group. The merging of data

according to the $\bar{3}m1$ point group led to the internal R value $R_{\text{int}} = 0.0625$ for all reflections. A first partial solution was found with direct methods as implemented in SHELXL97 (Sheldrick 1997). It was soon realized that some atoms were highly disordered and, accordingly, split atoms were successively added at the positions found in the Fourier difference syntheses. However, with such a model and regardless of the number of additional atoms it was not possible to obtain a residual value lower than ca. $R = 0.09$. The symmetry of the RT-structure of fettelite was previously reported as monoclinic (Bindi et al. 2009). A monoclinic solution with concomitant twinning laws was thus investigated by using JANA2006 (Petricek et al. 2006). Many trials involving various structure/space group combinations were tested, without any improvement of the F_{obs} vs. F_{calc} agreement. Going back to the trigonal system, $P\bar{3}m1$ space group, a non-harmonic approach with a Gram-Charlier development of the Debye-Waller factor (Johnson and Levy 1974; Kuhs 1984) was then attempted. This with the aim to reduce the number of refined positions, which lowers the correlation level, and thus may reach a convergence toward a reasonable structure model. A major improvement was achieved by introducing up to fourth order tensors for the Ag3 and Ag5 positions. A stable, non correlated model for the silver diffusion path was then found by using only three silver positions: Ag4 with regular anisotropic atomic displacement parameters and Ag3 and Ag5 with higher order tensors up to the fourth order. The residual R value converged smoothly to $R = 0.0285$ for 1004 reflections [$I > 2\sigma(I)$] and 76 parameters. Experimental details are given in Table 2 while atomic parameters are listed in Tables 3 to 5. A CIF is on deposit¹.

¹ Deposit item AM-11-025, CIF. Deposit items are available two ways: For a paper copy contact the Business Office of the Mineralogical Society of America (see inside front cover of recent issue) for price information. For an electronic copy visit the MSA web site at <http://www.minsocam.org>, go to the *American Mineralogist* Contents, find the table of contents for the specific volume/issue wanted, and then click on the deposit link there.

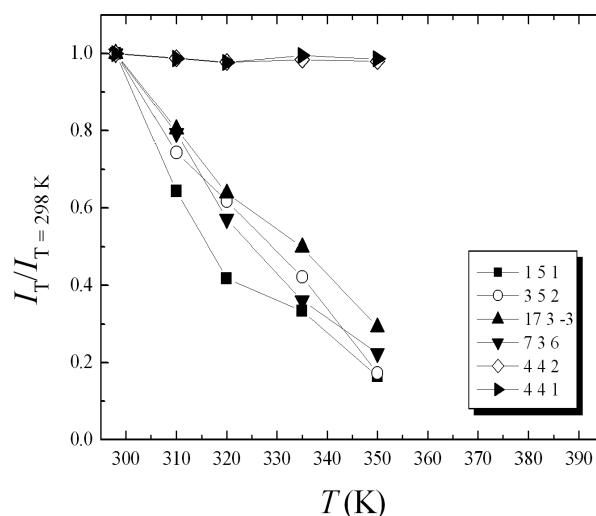


FIGURE 1. Temperature dependence of the relative intensity of some selected reflections for fettelite normalized to the value measured at 298 K. The intensity of reflections having h and $k = 2n + 1$ becomes very weak when the temperature increases, whereas that of reflections having h and $k = 2n$ remains constant.

TABLE 1. Unit-cell parameters for the selected fettelite crystal at different temperatures

T (K)	a (Å)	b (Å)	c (Å)	β (°)	V (Å ³)
298	26.042(2)	15.066(1)	15.535(1)	90.45(2)	6095(1)
310	26.111(3)	15.101(2)	15.542(2)	90.40(3)	6128(2)
320	26.194(4)	15.130(3)	15.546(3)	90.31(2)	6161(4)
335	26.245(3)	15.152(2)	15.550(3)	90.19(3)	6184(4)
350	26.302(4)	15.183(2)	15.553(2)	90.05(2)	6211(3)
400	7.5984(6)	7.5984(6)	15.557(2)	90.00	777.9(1)

RESULTS AND DISCUSSION

Description of the HT crystal structure

The HT-crystal structure of fettelite is topologically identical to that observed at room temperature (Table 6; Bindi et al. 2009). It consists of a regular succession of two module layers stacked along the *c*-axis: a first module layer (labeled *A*) with composition $[Ag_6As_2S_7]^{2-}$ and a second module layer (labeled *B*) with composition $[Ag_6(Ag,Hg)_5(As,Sb)_2S_8]^{2+}$. The disorder occurs in module *B* (Fig. 2). This modular approach does not imply that the layers are connected by van der Waals bonds. It is designed only for convenience and the analysis of each module cannot be made independently as some atoms have coordinating atoms in the other module.

The *A* module layer of fettelite (either at RT or HT) is identical to that described for the minerals belonging to the pearceite-polybasite group (see Fig. 2 of Bindi et al. 2009). The

arrangement of atoms in the *B* module layer is more complicated. In the HT structure, the silver/mercury cations are distributed along the diffusion path as illustrated in Figure 3. Using a non-harmonic description of the Debye-Waller factors, three Ag atom positions (Ag3 and Ag5 with non-harmonic atomic displacement parameters and Ag4 with classical atomic displace-

TABLE 2. Details pertaining to the single-crystal X-ray data collection and structure refinement at 400 K of fettelite from Chile

Crystal data	
Space group	$\bar{P}3m1$ (no. 164)
Cell parameters	$a = 7.5984(6)$ (Å) $c = 15.557(2)$ (Å) $V = 777.9(1)$ (Å ³)
Z	1
Crystal color	red
Crystal shape	platy
Crystal size (mm)	$0.095 \times 0.088 \times 0.012$
Data collection	
Diffractometer	Oxford Diffraction Excalibur 3
Radiation type	MoK α ($\lambda = 0.71073$)
Monochromator	oriented graphite (002)
Scan mode	φ/ω
Temperature (K)	400
Detector to sample distance (cm)	5
Number of frames	1125
Measuring time (s)	60
Maximum covered 2θ (°)	69.20
Range of h, k, l	$-11 \leq h \leq 11, -11 \leq k \leq 11, -24 \leq l \leq 24$
Collected reflections	13836
R_{int}	0.0625
Refinement	
Refinement coefficient	F^2
No. of refl. in refinement	1219
No. of observed refl.	1004
No. of refined parameters	76
Weighting scheme	$w = 1/[\sigma^2(I) + (0.044 \times I)^2]$
R_{obs}/R_{all}^*	0.0285/0.0302
wR^{2*} (obs)/ wR^{2*} (all)	0.0302/0.0303
Diff. Fourier (e ⁻ /Å ³)	[-0.58, 0.71]

$$* R = \frac{\sum ||F_o| - |F_c||}{\sum |F_o|}; wR^2 = \frac{[\sum w(|F_o|^2 - |F_c|^2)^2 / \sum w(|F_o|^2)]^{1/2}}{\sum w|F_o|^2}$$

TABLE 3. Wyckoff positions, site occupation factors, fractional atomic coordinates, and equivalent isotropic displacement parameters (Å²) for the selected fettelite crystal at 400 K

Atom	Wyckoff	s.o.f.	x	y	z	U_{iso}
Ag1	6i	1.00	0.46798(4)	0.53202(4)	0.30158(3)	0.0475(2)
Ag2	6i	1.00	0.29657(9)	0.14829(4)	0.08926(4)	0.0613(2)
Ag3	3f	0.854(5)	0.5	0	0.5	0.077(2)
Ag4	6h	0.20(1)	0.275(2)	0	0.5	0.040(2)
Ag5	6h	0.33(1)	0.201(2)	0	0.5	0.080(4)
As1	2d	1.00	0.3333	0.6667	0.07345(4)	0.0283(2)
As2	2c	0.776(3)	0	0	0.28096(3)	0.0288(2)
Sb2	2c	0.224	0	0	0.28096(3)	0.0288(2)
S1	6i	1.00	0.4840(1)	0.5160(1)	0.1430(1)	0.0587(8)
S2	6i	1.00	0.3033(2)	0.15166(8)	0.35386(5)	0.0288(3)
S3	2d	1.00	0.3333	0.6667	0.43642(8)	0.0288(4)
S4	1a	1.00	0	0	0	0.090(2)

TABLE 4. Anisotropic displacement parameters U_{ij} (Å²) for the selected fettelite crystal at 400 K

Atom	U_{11}	U_{22}	U_{33}	U_{12}	U_{13}	U_{23}
Ag1	0.0454(2)	0.0454(2)	0.0412(2)	0.0149(2)	-0.00711(8)	0.00711(8)
Ag2	0.0451(3)	0.0615(3)	0.0718(3)	0.0225(1)	-0.0365(2)	-0.0183(1)
Ag3	0.138(4)	0.028(1)	0.0277(9)	0.0141(6)	0.0003(3)	0.0005(6)
Ag4	0.053(4)	0.035(2)	0.026(2)	0.0173(9)	0.0096(7)	0.019(1)
Ag5	0.103(7)	0.096(4)	0.039(2)	0.048(2)	-0.0057(9)	-0.011(2)
As1	0.0353(2)	0.0353(2)	0.0143(2)	0.0176(1)	0	0
As2	0.0349(2)	0.0349(2)	0.0165(2)	0.0175(1)	0	0
Sb2	0.0349(2)	0.0349(2)	0.0165(2)	0.0175(1)	0	0
S1	0.081(1)	0.081(1)	0.0473(6)	0.066(1)	0.0020(2)	-0.0020(2)
S2	0.0318(5)	0.0309(3)	0.0239(3)	0.0159(2)	0.0017(3)	0.0008(2)
S3	0.0353(5)	0.0353(5)	0.0160(5)	0.0176(3)	0	0
S4	0.092(3)	0.092(3)	0.087(3)	0.046(2)	0	0

TABLE 5. Higher order displacement parameters*† for Ag3 and Ag5 atoms for the selected fettelite crystal at 400 K

	Ag3	Ag5
C^{111}	0	0.062(18)
C^{112}	0	-0.008(5)
C^{113}	0	0.0015(8)
C^{122}	0	-0.008(5)
C^{123}	0	0.0015(8)
C^{133}	0	-0.0009(4)
C^{222}	0	0
C^{223}	0	0
C^{233}	0	0
C^{333}	0	0
D^{1111}	0.012(9)	0.05(2)
D^{1112}	-0.0007(2)	-0.007(6)
D^{1113}	-0.0005(3)	0.0020(9)
D^{1122}	-0.0001(1)	-0.004(5)
D^{1123}	-0.0003(2)	0.0012(6)
D^{1133}	0.00002(1)	-0.0008(3)
D^{1222}	0.001(4)	0.003(2)
D^{1223}	0.0001(8)	0.000(3)
D^{1233}	-0.00003(2)	-0.0004(1)
D^{1333}	0.00003(2)	-0.00006(5)
D^{2222}	0.002(9)	0.01(4)
D^{2223}	0.0001(2)	-0.001(5)
D^{2233}	-0.00007(5)	-0.0007(3)
D^{2333}	0.00007(3)	-0.00012(1)
D^{3333}	0.00001(3)	-0.00002(6)

* Third-order tensor elements C^{ijk} are multiplied by 10^3 .

† Fourth-order tensor elements D^{ijkl} are multiplied by 10^4 .

TABLE 6. Main interatomic distances (Å) for the selected fettelite crystal at 400 K

	As1-S1	As2-S2	Ag1-S1	Ag1-S2
As1-S1	2.259(1)	2.296(1)	2.476(2)	2.639(1)
As1-S2	2.259(1)	2.296(1)	2.639(1)	2.639(1)
<As1-S>	2.259	2.296	Ag1-S3	2.746(1)
Ag2-S1	2.560(1)	Ag3*-S3	<Ag1-S>	2.625
Ag2-S1	2.560(1)	Ag3-S3	Ag4-S2	2.509(2)
Ag2-S4	2.395(1)	<Ag3-S>	Ag4-S2	2.509(2)
<Ag2-S>	2.505	2.406	Ag4-S3	2.950(7)
Ag5*-S2	2.491(2)		Ag4-S3	2.950(7)
Ag5-S2	2.491(2)		<Ag4-S>	2.730
<Ag5-S>	2.491			

* The distances for Ag3 and Ag5 correspond to the most probable distance calculated from the modes (maxima) of joint probability density function (jpdf) maps.

ment parameters) are sufficient for the density modeling of the diffusion path, including the interconnection between the rings. The model is validated by the small negative value in the joint probability density function. Mercury does not have a specific ordered position at high temperature. Nevertheless, the overall mean electron number of the *B* module layer excluding As and S is 550 electrons for the RT structure (corresponding to 10Ag and 1 Hg) and 552 electrons for the HT structure (Table 3), which indicates an excellent match.

DSC and conductivity measurement analysis

The DSC curve in Figure 4 shows a clear peak at about 380 K indicating that a phase transition took place at this temperature. The Arrhenius plot of conductivity σ ($\log \sigma T$ vs. $1/T$ plot) is shown in Figure 5. Two conductivity domains are observed: a low-temperature region where the Arrhenius law,

$$\sigma(T) = \frac{\sigma_0}{T} \exp\left(\frac{E_a}{kT}\right)$$

is obeyed (i.e., a straight line is observed) and a high-temperature region where a deviation from the Arrhenius law is apparent. Change from one conductivity regime to the other one occurs at about 380 K where the phase transition was observed on the DSC curve (Fig. 4).

For the low-temperature domain the activation energy for conductivity is 0.43 eV, whereas the conductivity for the ordered

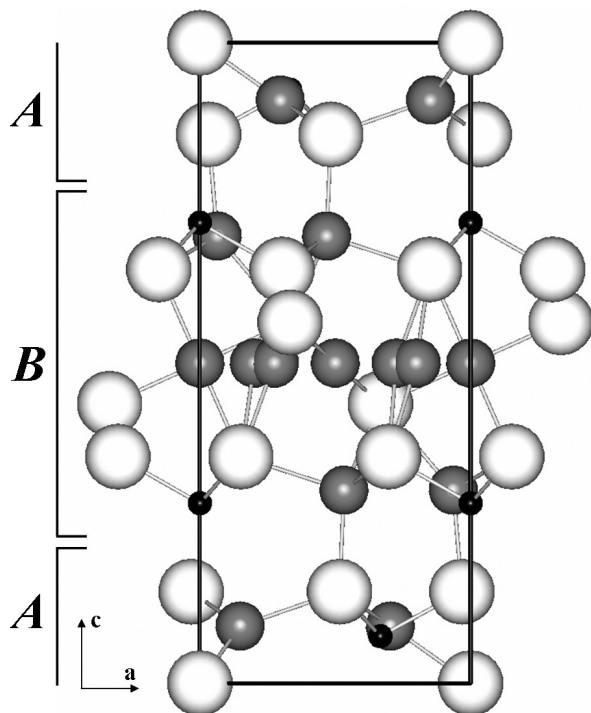


FIGURE 2. Projection of the HT-structure of fettelite along the hexagonal *a*-axis, emphasizing the succession of the $[Ag_6As_2S_7]^{2-}$ *A* and $[Ag_6(Ag,Hg)_5As_2S_8]^{2+}$ *B* module layers. Ag, As, and S atoms are drawn in dark gray, black, and white, respectively. The unit cell and the orientation of the figure are outlined.

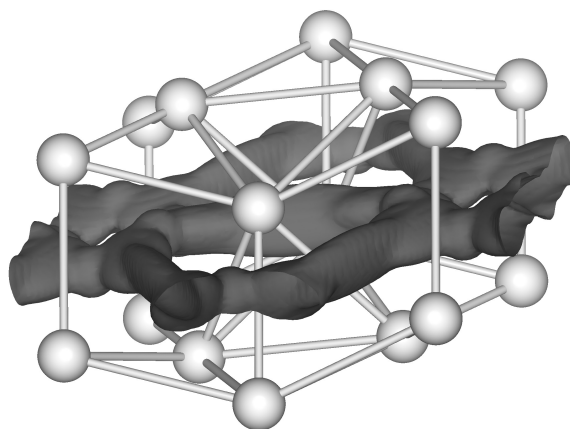


FIGURE 3. Non-harmonic joint probability density isosurface for Ag/Hg in the HT-structure of fettelite exhibiting the silver diffusion in the *a-b* plane. Part of the *B* layer extended with S atoms. Level of the map: 0.05 \AA^{-3} . Sulfur atoms in arbitrary size.

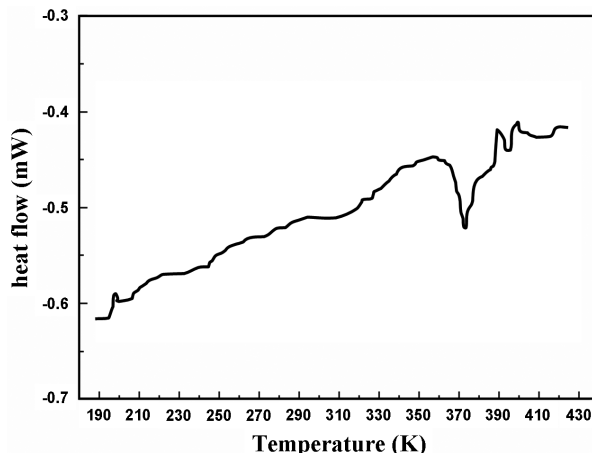


FIGURE 4. Differential scanning calorimetry curve for fettelite.

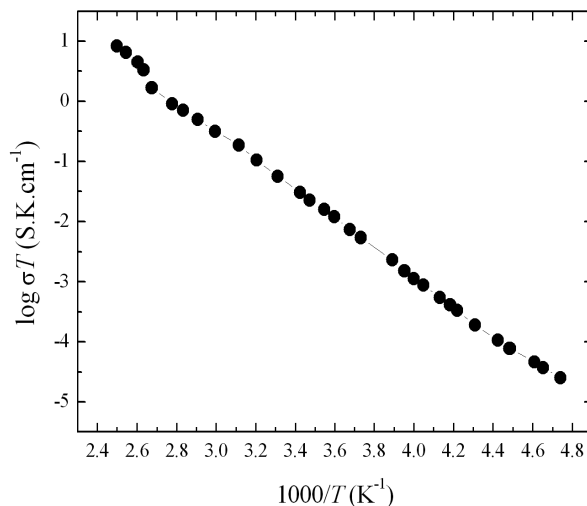


FIGURE 5. An Arrhenius plot of $\log(\sigma T)$ vs. $1000/T$ for fettelite.

phase is $5.0 \cdot 10^{-5} \text{ S cm}^{-1}$ at 250 K. At low temperature (and at RT as well), fettelite has locally ordered Ag sites within the *B* module layer (Bindi et al. 2009). A classical behavior for the conductivity (it obeys the Arrhenius law) is therefore expected with a similar activation energy.

At high temperature, the phase changes from an ordered structure to one where the Ag ions in the *B* module layer are disordered. A complete delocalization of Ag leading to a quasi-liquid displacement for this ion is observed (Fig. 3). As a result, the Arrhenius law is no longer observed. The limiting activation energy evaluated from the “apparently” linear part of conductivity in the high-temperature region is about 0.13 eV. The observed behavior is characteristic of superionic conductors that show a strong disorder in the sub-lattice of the moving cations.

Different polytypes of fettelite

As temperature is decreased (starting from the high-temperature structure), Ag cations adopt low potential, preferential sites. This setting requires both a larger cell and a lower symmetry, and results in an apparent hexagonal cell with the $2a \times 2a \times c$ parameters and the real $2a\sqrt{3} \times 2b \times c$ ($\beta = 90.48^\circ$) monoclinic cell with the *C2* space group observed at room temperature (Bindi et al. 2009). During the ordering process, second-order twinning usually takes place, which dramatically complicates the structure determination (see the detailed description of the complex twinning observed for fettelite at RT by Bindi et al. 2009).

As documented by Bindi et al. (2007), pearceite-polybasite minerals show three different unit-cell types: 111 (polytype-*Tac*), 221 (polytype-*T2ac*), and 222 (polytype-*M2a2b2c*), which represent the strongly disordered (space group $P\bar{3}m1$), partially ordered (space group *P321*), and fully ordered form (space group *C2/c*), respectively. By analogy, fettelite represents the fully ordered stable form at room temperature. It converts to a disordered form at high temperature, where the disorder gives rise to a folding of the cell along the **a**- and **b**-directions, as found in the 111 structures of the pearceite-polybasite minerals (Bindi et al. 2007). By analogy, it is very likely that different polytypes exist in nature depending upon the Ag/Hg ratio. The higher the Ag/Hg ratio, the greater the possibility of having the disordered polytype at room temperature. The situation is, however, more complicated than it appears from what reported in this paper. However disordering is not only created by the substitution of Hg

for Ag, but also by the substitution of Sb for As. If the substitution of Ag by Hg is of prime importance in the structure ordering, then that of Sb by As could be significant as well. In addition, it is possible that some fettelite, which contains small amounts of selenium substituting for sulfur, might form a different structure. Only a complete structure determination, including the structural effects produced by twinning, can resolve this question.

ACKNOWLEDGMENTS

We thank Annie Pradel for the DSC measurements on the fettelite sample. This work was funded by C.N.R. (Istituto di Geoscienze e Georisorse, sezione di Firenze) and by M.I.U.R., P.R.I.N. 2007 project “Complexity in minerals: modulation, phase transition, structural disorder.”

REFERENCES CITED

- Bindi, L., Evain, M., Pradel, A., Albert, S., Ribes, M., and Menchetti, S. (2006) Fast ionic conduction character and ionic phase-transitions in disordered crystals: The complex case of the minerals of the pearceite-polybasite group. *Physics and Chemistry of Minerals*, 33, 677–690.
- Bindi, L., Evain, M., Spry, P.G., and Menchetti, S. (2007) The pearceite-polybasite group of minerals: Crystal chemistry and new nomenclature rules. *American Mineralogist*, 92, 918–925.
- Bindi, L., Keutsch, F.N., Francis, C.A., and Menchetti, S. (2009) Fettelite, $[\text{Ag}_6\text{As}_2\text{S}_7][\text{Ag}_{10}\text{HgAs}_2\text{S}_8]$ from Chañarcillo, Chile: Crystal structure, pseudo-symmetry, twinning, and revised chemical formula. *American Mineralogist*, 94, 609–615.
- Gaudin, E., Boucher, F., and Evain, M. (2001) Some factors governing Ag^+ and Cu^+ low coordination in chalcogenide environments. *Journal of Solid State Chemistry*, 160, 212–221.
- Johnson, C.K. and Levy, H.A. (1974) In *International Tables for X-ray Crystallography*, vol. IV, p. 311–336. Kynoch Press, Birmingham.
- Kuhs, W.F. (1984) Site-symmetry restrictions on thermal-motion-tensor coefficients up to rank 8. *Acta Crystallographica*, A, 40, 133–137.
- Owens, B.B. and Argue, G.R. (1967) High-conductivity solid electrolytes: MAG_4I_5 . *Science*, 157, 308–310.
- Oxford Diffraction (2006) CrysAlis RED (Version 1.171.31.2) and ABSPACK in CrysAlis RED. Oxford Diffraction, Abingdon, Oxfordshire, England.
- Petricek, V., Dusek, M., and Palatinus, L. (2006) JANA2006, Structure Determination Software Programs. Institute of Physics, Academy of Sciences of the Czech Republic, Prague, Czech Republic.
- Reuter, B. and Hardel, K. (1965) Silbersulfidbromid Ag_3SBr und Silbersulfidjodid Ag_3SI . I. Darstellung, Eigenschaften und Phasenverhältnisse von Ag_3SBr und Ag_3SI . *Zeitschrift für Anorganische und Allgemeine Chemie*, 340, 158–167.
- Sheldrick, G.M. (1997) SHELXL-97. A program for crystal structure refinement. University of Göttingen, Germany.